Roman double-layered crucibles from Autun/France: a petrological and geochemical approach

Daniela König*, Vincent Serneels

Department of Geosciences, University of Fribourg, Chemin du Musée 6, CH-1700 Fribourg, Switzerland

Eighteen double-layered crucible fragments found in an archaeological excavation site of the Lycée militaire (Autun/France), which dates to the Gallo-Roman period, were analysed with a series of classical mineralogical techniques in order to obtain knowledge about the raw materials of the individual layers. This work focuses on the usage of the crucibles as well as technical aspects of their production. The crucible fragments were studied by using petrographical (optical microscopy), elemental (SEM-EDS, EMPA, XRF-WDS) and mineralogical (XRD) techniques.

The two main layers of the crucibles are made of high refractory, kaolinite-based ceramic with granite-related temper grains. The analytical and petrographical results show remarkable differences between these two layers. The outer one is dominated by a high content of vitrified mullite-bearing matrix and contains analcime which was formed during the burial stage. In contrast, the inner layer is characterised by a non-vitrified matrix with a high content of orthorhombic mullite, β-cristobalite and α-quartz. An engobe is detectable in the majority of the fragments. The mineral composition allows an estimation of the firing temperatures, which have reached approximately 1200 up to 1400 °C.

1. Introduction

Crucibles and moulds from archaeological excavations are tools indicating specific metalworking practices of a certain period and bearing a large amount of information concerning the local metalworking, i.e. metal composition, production routine, etc. (e.g. Nielen, 2006; Tite et al., 1985).

Former studies generally distinguish between three functional groups of metalworking crucibles, namely cementation, assaying and melting crucibles (e.g. Bayley and Rehren, 2007). Melting crucibles are the most common type and are known since the Late Neolithic (Bayley and Rehren, 2007). It was necessary to construct them small but strong in order to guarantee easy handling of such metal charged vessels. Accordingly, the volume was commonly limited typically to a maximum of one litre of liquid metal, but often much less, prior to the Industrial Revolution. Such an usage also requires a fabric which ensures mechanical stability at temperatures well above 1000 °C (Bayley, 1992; Bayley and Rehren, 2007).

Individual crucibles show different fabric and material characteristics according to their special function. Bayley and Rehren (2007) classify crucibles using three main attributes: firstly, features related to the crucible design (e.g. shape and size), secondly, the ceramic fabric including mineralogical and structural features and thirdly, the technical function. One milestone in the development of crucibles is the usage of refractory materials, mainly white-firing kaolinitic clays. These materials first arose in the Late Iron Age, became a major component of crucibles during the Roman period, but their complete technical potential was only developed during the medieval period (Bayley and Rehren, 2007; Freestone, 1989; Martinón-Torres et al., 2008; Rehren, 2003; Thornton and Rehren, 2009). A common type of Roman crucible is characterised by a double-layered wall structure. Some authors suggest an insulation function of the outer layer which can give off heat more equally, thus reducing the probability of a thermal shock (e.g. Bayley and Rehren, 2007).

This article is a petrological and geochemical approach to identify and classify the metalworking crucibles from Autun/France. Individual aims are: (1) the detailed understanding of the ceramic structure and the investigation of the mineralogical/geochemical composition of the two main layers; (2) the characterisation of a potential engobe with regard to function and characteristics; (3) the identification of multiple usages; (4) the calculation of mineral-related firing temperatures; (5) the understanding of the production processes of the crucibles.

* Corresponding author. Tel.: +41 (0)263008946; fax: +41 (0)263009742.
   E-mail address: daniela.koenig@unifr.ch (D. König).

2. Double-layered crucibles from Autun

The modern town of Autun/France (Fig. 1) developed from the Roman town of Augustodunum, one of the most important settlements in Gaul. Excavations at the site of the Lycée militaire have brought to light a craftsman district dominated by copper-based metalworking. More than 50 workshops were producing between the 1st and 3rd century A.D. (Chardron-Picault and Pernot, 1999).

Large quantities of crucible fragments (650 kg) and lids, and in few cases completely preserved crucibles (Fig. 2), were found in the area of the Lycée militaire. Preserved and reconstructed crucibles occur in slightly different shapes and at least three sizes with a volumetric capacity between 0.3 and 2.2 L, i.e. 2.5−19 kg metallic charge. The crucible shapes are mainly cylindrical with a hemispherical base and some of them show a tapering shape to the top. Main types are reclosable with a separate lid and without any spout. This design is almost identical for all crucibles sizes.

3. Analytical approach

In order to have a representative selection of sample material, eighteen crucible fragments were selected from the excavation part US 1534 (see Chardron-Picault and Pernot, 1999). Fabric studies were made on polished thin-sections by using a polarising microscope and a "FEI SIRION XL 30S FEG" scanning electron microscope (SEM). Secondary electron (SE) and back-scattered images (BSE) were recorded with an acceleration potential of 20−25 kV, a beam current of 1.2 nA, a working distance of 8 mm and a measuring time of 50 s per point. Semi-quantitative chemical analyses were obtained by energy dispersive spectrometry (EDS) with an "EDAX NEW-XL30" detector. Cross-section scans were used to generate X-ray maps of the elements Al, Na, Mg, Si, P, K, Sn, Ca, Ti, V, Mn, Fe, Cu and Zn (25 kV−1.2 nA, dwell time 50 ms per pixel). The engobe were quantitatively analysed with a "JEOL JXA-8200" electron microprobe at the University of Bern (15 kV−20 nA, 5 μm spot size).

Where possible, both main layers were manually separated and milled in a tungsten carbide pot using a vibratory disc mill. The total amount of sample material varied between 3 and 8 g, depending on layer thickness and the size of the crucible fragment. X-ray diffraction (XRD) analyses were obtained from a "PHILIPS PW1800"
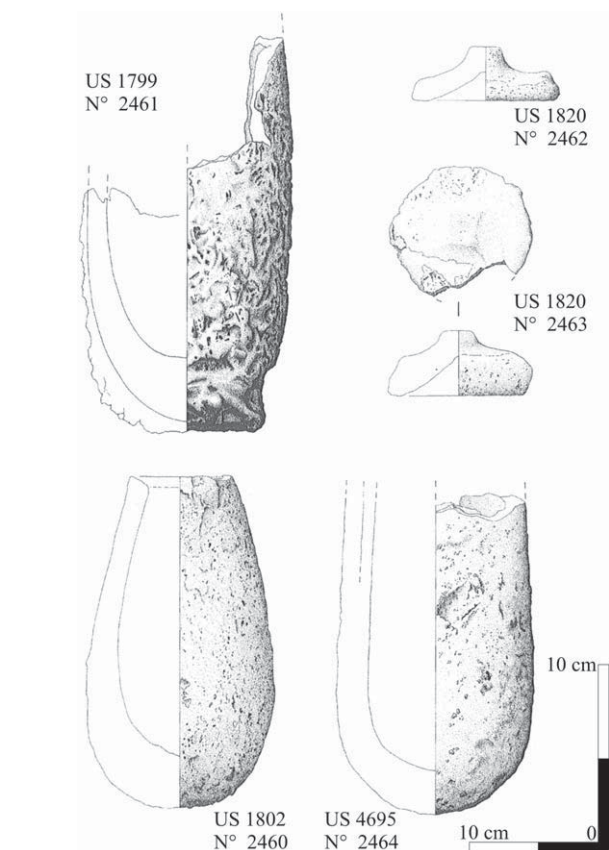
Fig. 2. Drawings of three representative crucible shapes from Autun; US 1799, N° 2461 − inner diameter: 11.5 cm, metal load: 21 cm; US 1802, N° 2460 − inner diameter: 9.5 cm, metal load: 18 cm; US 4695, N° 2464 − inner diameter: 10.3 cm, metal load: 18 cm (modified after Chardron-Picault and Pernot, 1999).

diffractometer with CuKα radiation at 40 kV−40 mA (0.02 °2Θ/step, 5 s/step, 5−90 °2Θ). To determine the exact position of the (101)-peak of cristobalite, a silicon standard was measured after each tenth sample.

Bulk chemical analyses were carried out with a "PHILIPS PW 2400" X-ray fluorescence wavelength dispersive spectrometer (XRF-WDS). All analyses were performed on pressed powder discs, which were prepared with 2.5−5 g of sample material and evaluated with the program "uniquant". The disc diameter is constant (32 mm), although thicknesses can vary as a function of the sample amount. Very thin discs were pressed twice with boric acid to guarantee definite stability during the measuring procedure. The loss on ignition (LOI) was estimated with the help of a "Mettler-Toledo TGA/SDTA 851e" thermogravimetry device (TGA). Raman spectroscopy was carried out on an "Olympus BX40" spectroscope (370 mW, 25 A) equipped with a green laser.

4. Results and discussion

In general, all studied crucibles from Autun show a double-layered wall structure as exemplarily shown in Fig. 3. Individual layers possess their own thicknesses and fabric characteristics. The thickness of the outer layer increases from top to bottom, while the inner one remains nearly constant (Table 1; Fig. 3). Outer and inner layers can optically be distinguished by their different colours and the vitrified/non-vitrified appearance. These optical features indicate mineralogical heterogeneities between single layers and individual fragments. The inner layer is covered by an added engobe (see Section 4.2) as already reported from other excavations

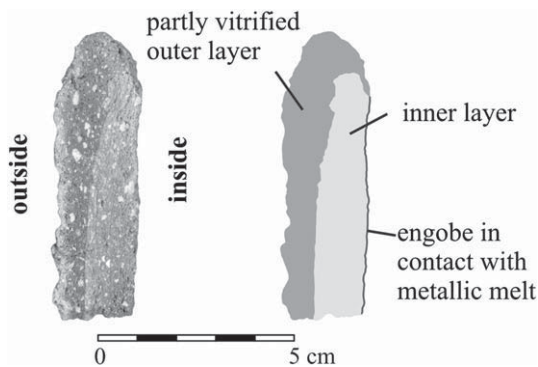Fig. 1. Map of France with Autun in.

2

Fig. 3. Photograph of sample ATM 005 (left) and a sketch (right) of its main structural units.

like Neuss and Eberdingen-Hochdorf (Modarressi-Tehrani, 2004; Nielen, 2006). The outer, highly vitrified surface shows charcoal imprints implying heating from below. Copper-related colours (red and green) on the outer surface of the outer layer result from varying redox conditions during the metal-melting process in the furnace.

4.1. Geochemical and mineralogical characterisation of the two main layers

Macroscopically as well as microscopically it is possible to separate the layers with respect to their porosity, colour, grade of vitrification and the number and size of temper (Figs. 4 and 5). Observable matrix variations between both layers are linked to chemical and mineralogical variations. Temper grains consisting of quartz, feldspar and minor amounts of mica. Their proportions differ between the main layers of the investigated fragments. The outer layer consists of 60−70% temper grains dominated by potassium feldspar over quartz. In contrast, the inner layer possesses a total of 40−50% temper grains with nearly equal amounts of potassium feldspar and quartz. Generally, temper grains are sharp edged and vary in size between tens of micrometres and some millimetres. The low amount of detectable mica flakes has no influence on thermal stability.

The outer layer shows a much higher porosity than the inner one, which is a direct consequence of its high degree of vitrification. During the firing process pore volume and size steadily increase

until a maximum porosity is reached at a temperature around 950 °C−1050 °C (Maggetti and Kahr, 1980; May and Butterworth, 1962). A closed porosity within the glassy matrix is a common feature observed in all fragments of the outer layer. In contrast, the inner layer shows a semi-open porosity. These pores are a result of a thermally induced dehydroxylation and subsequent phase transformation of kaolinite to mullite during firing in the furnace and are not related to an addition of fibrous organic material.

SEM investigations show remarkable differences within the two main layers and the engobe, namely in texture (vitrified/non-vitrified). Moreover, calcium element maps and line measurements are suited to show major differences in bulk chemistry along the wall section. The border between the main layers as well as the engobe is marked by a significant change in the calcium content (Fig. 6). Moreover, the engobe is characterised by an appearance of metal droplets consisting of copper−tin or copper−zinc alloys (unpublished data). Additionally, element migration (Zn) related to the metal-melting process is observable along the inner layer. SEM-BSE investigations are also suited to distinguish between primary mullite within the vitrified matrix and micrometre sized acicular secondary mullite in direct contact to potassium feldspar grains (Fig. 7) (Lee and Iqbal, 2001).

Based on XRD analyses (Table 1) quartz, mullite, potassium feldspar and cristobalite have been identified as the main constituents of both layers, accompanied by minor amounts of analcime in the outer layer. The amplitudes and the broadness of cristobalite peaks as well as a high background in the 40−55 °2Θ region indicate weak crystallinity and a high amount of glassy material within the outer layer of the ceramics. XRD detectable analcime is a typical alteration product of the vitrified phase developed in ceramics fired at high temperature (Pradell et al., 2010).

XRF bulk data verifies the chemical heterogeneities between both main layers. Table 2 summarises semi-quantitative data of the major components of the crucibles and indicates a dominance of SiO_2 and Al_2O_3, followed by K_2O in the inner and CaO in the outer layer, respectively. The content of alkali earth elements is mainly attributed to the matrix and the feldspar remnants therein. TG analyses yield a LOI of less than 0.2 wt.% within the ceramics. This is the result of a relatively high firing temperature. However, LOI does not wholly account for the deviation of the total sum of the elements, which is in fact due to the utilisation of pressed powder discs, instead of more accurately measurable glass discs (Table 2).

The compositional variations of the main layers are also visible in diagrams of Al_2O_3−SiO_2, MgO−SiO_2, CaO−SiO_2 and K_2O−SiO_2,

Table 1
Crucible thickness and qualitative mineral content of both layers (i − inner layer; o − outer layer) determined by XRD; some specimens could not be separated.

Sample	Thickness (mm) bulk (in; out)	Existence of the engobe	d_{101} Crs (nm)	Mineral content − inner layer	Mineral content − outer layer
ATM 001	19 (12; 7)	x	0.4062	Qtz + Crs + Mul + Or	Qtz + Crs + Mul + Anl
ATM 002	16 (12; 4)	x	0.4060	Qtz + Crs + Mul + Or	Qtz + Crs + Mul + Anl
ATM 003	16 (6−12; 10−4)	(x)	−	Qtz + Mul + Lct	Qtz + Mul
ATM 004	20 (10; 10)	x	0.4065	Qtz + Mul + Or	Qtz + Crs + Mul
ATM 005	21 (8−12; 13−9)	(x)	0.4062	Qtz + Crs + Mul	Qtz + Crs + Mul + Anl + Spl
ATM 006	17 (10; 7)	x	0.4059	Qtz + Crs + Mul + An	Qtz + Crs + Mul + Anl + An
ATM 007	15 (9−12; 6−3)	(x)	0.4063	Qtz + Crs + Mul + Lct + Anl	
ATM 008	26−35 (20−23; 15−3)	x	0.4058	Qtz + Crs + Mul + Or	Qtz + Crs + Mul + Anl
ATM 009	37−69 (22; 15−47)	x	0.4061	Qtz + Crs + Mul + Or	Qtz + Crs + Mul
ATM 010	40 (21; 19)		0.4059	Qtz + Crs + Mul	Qtz + Crs + Mul + Anl + Or
ATM 011	45 (20; 25)		0.4060	Qtz + Crs + Mul + Or	Qtz + Crs + Mul + Anl + Or
ATM 012	16−20 (11−12; 9−4)	x	0.4059	Qtz + Crs + Mul + Anl	
ATM 013	23 (15; 8)	x	0.4058	Qtz + Crs + Mul	Qtz + Crs + Mul + Anl
ATM 014	22 (18; 5)	x	0.4058	Qtz + Crs + Mul	Qtz + Crs + Mul + Anl
ATM 015	21−25 (11−15; 10)	x	−	Qtz + Crs + Mul + Anl	
ATM 016	18 (12−15; 6−3)	x	0.4059	Qtz + Crs + Mul + Or	
ATM 017	20−24 (15−17; 5−7)	x	0.4061	Qtz + Crs + Mul	Qtz + Crs + Mul + Anl + An
ATM 018	42 (22; 20)		−	Qtz + Mul + Or	Qtz + Crs + Mul + Anl

Mineral abbreviations: quartz (Qtz); cristobalite (Crs); mullite (Mul); analcime (Anl); orthoclase (Or); spinel (Spl); anorthite (An); leucite (Lct).
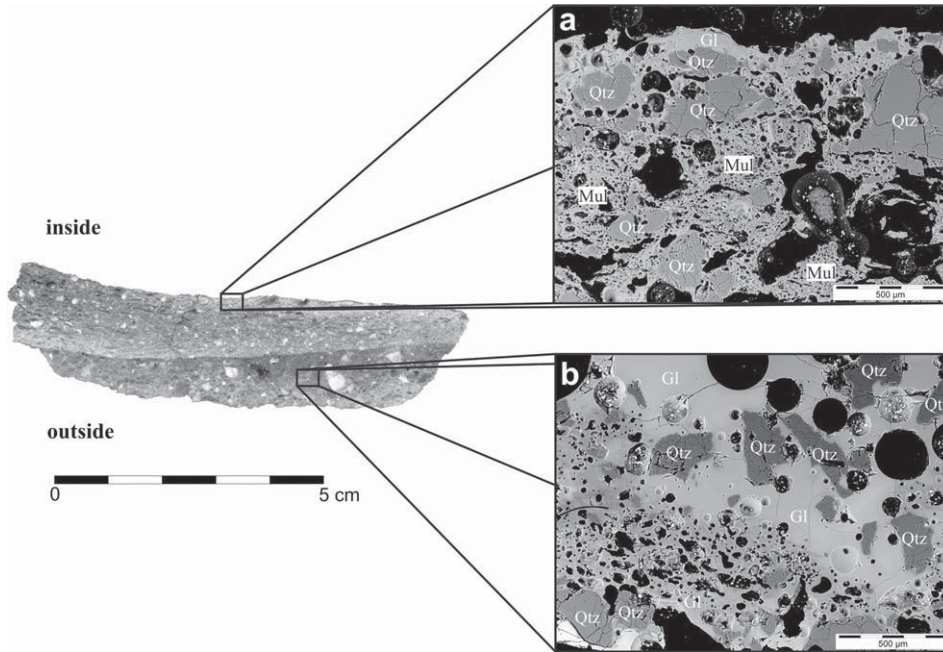
Fig. 4. Left: representative section through the crucible fragment ATM 004, which illustrates both main layers with different colour and fabric characteristics; right: SEM-BSE images representing the differing fabric characteristics of the inner (a) and outer (b) layer; Qtz − quartz; Mul − mullite; Gl − glass.

which allow a clear distinction (Fig. 8). The outer layer contains a higher amount of CaO, MgO, K_2O and Fe_2O_{3tot} than the inner one. The content of Al_2O_3 behaves contrariwise. The binary plots of SiO_2/Al_2O_3−CaO, SiO_2/Al_2O_3−MgO, Fe_2O_{3tot}/Al_2O_3−CaO and Fe_2O_{3tot}/Al_2O_3−MgO point toward two distinguishable clay types (Fig. 9).

The above-mentioned results lead to a similar outcome and interpretation, namely that the inner and outer layers are different.

In general, it is possible to argue with two reasons for the present ceramic properties. Firstly, the differences in porosity and the total amount of vitrified matrix directly correspond to the chosen production routine. A second, but not less important cause is related to the kind of usage, i.e. the way the crucibles were used for the melt production, which had a direct impact on the observed zinc migration within the wall sections. The inner layer is made up
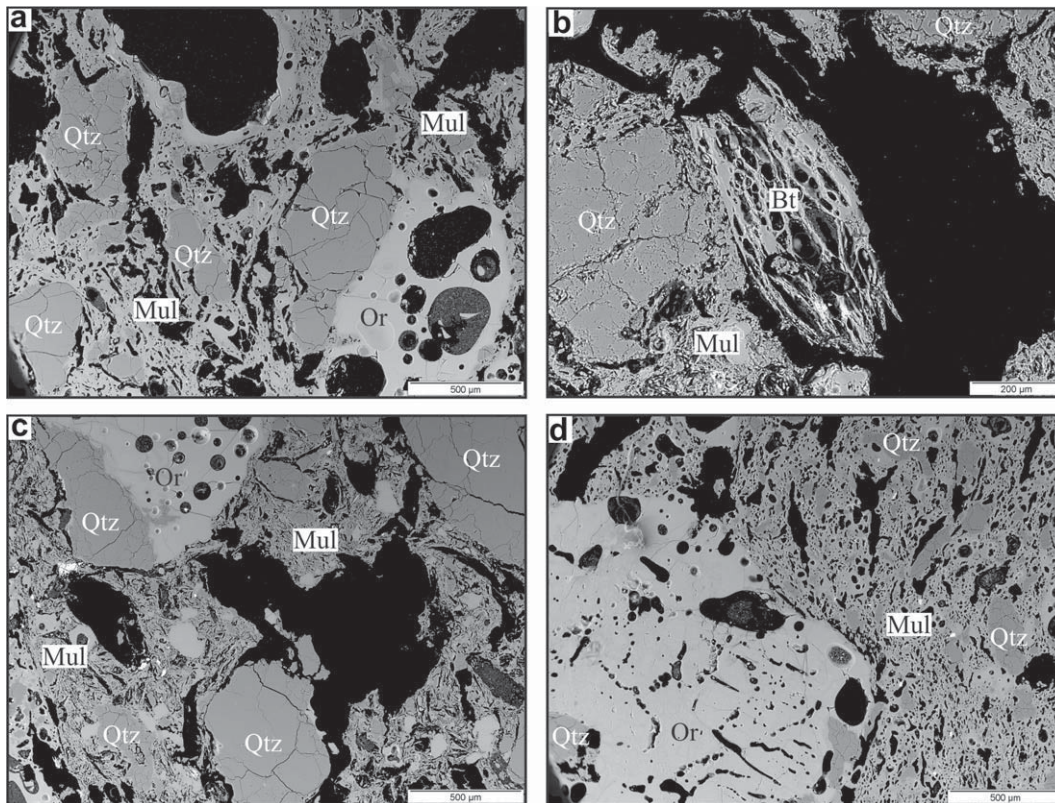

Fig. 5. (a−d) SEM-BSE images showing different types of temper grains within the inner layer; Qtz − quartz; Mul − mullite; Or − orthoclase; Bt − biotite.
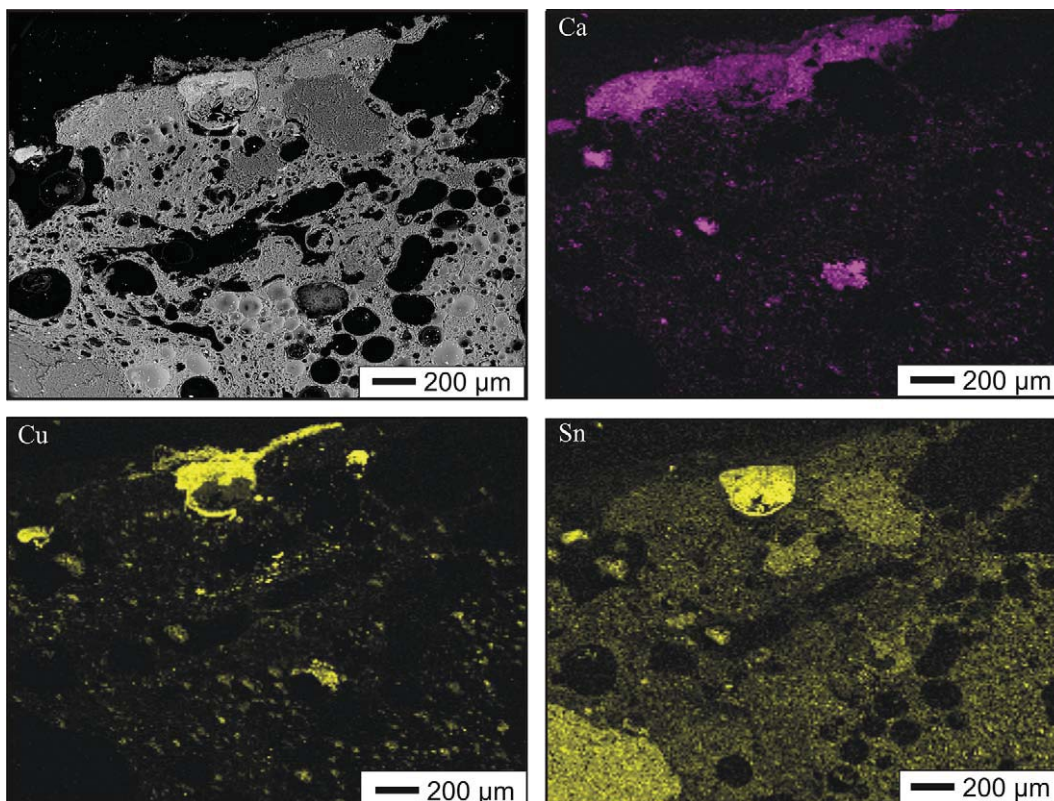
4

Fig. 6. SEM-BSE image and element maps showing the engobe with high calcium content compared to the inner layer; copper and tin maps showing the metal droplets within the engobe; the bright area in the left corner of the tin map corresponds to an measurement artifact (overlap of SEM-EDS Si line and Sn line).

of 50% non-vitrified matrix (mainly mullite), and 50% temper grains, which are composed of even amounts of quartz and feldspar, which are often intergrown (Fig. 5). In contrast, the outer layer is made up of 40% vitrified matrix containing mullite and analcime, and 60−70% temper grains consisting of more feldspar than quartz. Thus, the ceramics are predominantly composed of granite-related temper grains hosting in an orthorhombic mullite-bearing matrix which was formed by the dehydroxylation of kaolinite as well as the stepwise phase transformation to mullite, primarily initiated by the firing process. The outer layer has a slightly different chemical composition related to a marly limestone, marl or ash additive. A more detailed specification of the calcium additive was not yet possible due to missing sediment grains or locally enriched phosphate traces. However, anyone of these additives would have been

Fig. 7. SE image of acicular secondary mullite surrounded by a matrix of primary mullite.

used to increase the calcium and magnesium content in order to obtain a glassy layer. A primary calcium enriched kaolinitic clay can be excluded, cause of a general rareness of such clays in nature. The use of two different kaolinitic clays implies detailed knowledge of the chemical composition of different clay types, which can be excluded for Roman times. In general, the complete mineral composition of the investigated crucibles allows conclusions about firing and collapse temperatures, which will be discussed in Section 4.4.

An outer layer resulting from a reaction with fuel ash components can be excluded, because of a missing reaction rim. Calcium and magnesium are evenly distributed in the outer layer, i.e. there exist no detectable diffusion front. Furthermore, the measured magnesium content is too low for a mid-European fuel ash mainly produced from hardwood with quite higher magnesium contents. In addition, there is a sharp boarder between both layers resulting from chemical and compositional differences (Fig. 3). Moreover, the binary plots in Fig. 9 reflecting the clay composition point towards two different clay sources.

4.2. The engobe as a kind of inner protecting layer

The engobe is preserved in the majority of the investigated fragments and has an average thickness of 100 μm (Table 1; Fig. 10). Almost all preserved metal droplets of the investigated crucibles are distributed on top of remnants of this protecting layer and not within the semi-open porosity of the inner layer except of crack related porosity.

Besides SEM-EDS and EMPA, the engobe was analysed by Raman spectroscopy to gather additional data. XRD and XRF-WDS analysis were not performed owing to low sample amounts. However, Raman data yield no evidence for a charcoal based layer or fuel ash
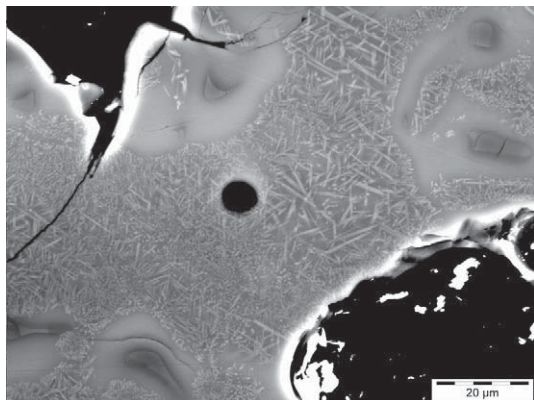
Table 2
Semi-quantitative bulk chemical data of the crucibles separated after layer (XRF-WDS); shaded − main metallic charge material.

| Sample		SiO$_2$ (wt.%)	TiO$_2$ (wt.%)	Al$_2$O$_3$ (wt.%)	Fe$_2$O$_{3tot}$ (wt.%)	MnO (wt.%)	MgO (wt.%)	CaO (wt.%)	Na$_2$O (wt.%)	K$_2$O (wt.%)	P$_2$O$_5$ (wt.%)	Sum norm. (wt.%)	Sum before norm. (wt.%)	Ba (ppm)	Cr (ppm)	Cu (ppm)	Pb (ppm)	Sn (ppm)	Sr (ppm)	Zn (ppm)
ATM 001	In	68.5	0.7	23.9	1.8	0.02	0.6	0.5	0.4	3.5	0.3	100	99.1	1000	38	1320	29	230	<100	3960
	Out	69.2	0.7	15.3	3.1	0.07	0.8	4.3	1.2	4.8	0.7	100	94.1	1390	75	768	32	16	118	1010
ATM 002	In	72.8	0.6	20.8	1.3	0.02	0.4	0.3	0.3	3.2	0.2	100	93.5	1410	31	259	46	22	<100	3580
	Out	67.6	0.6	19.0	1.7	0.13	0.9	4.8	0.4	4.5	0.3	100	94.7	3140	42	810	54	9	205	1540
ATM 003	In	72.2	0.7	20.3	2.0	0.04	0.4	0.3	0.4	3.2	0.3	100	94.3	1110	31	451	50	46	<100	25,500
	Out	74.6	0.6	15.7	2.4	0.07	0.7	1.0	0.8	4.0	0.3	100	96.3	1400	48	969	30	43	105	2650
ATM 004	In	68.6	0.7	23.6	1.6	0.02	0.5	0.4	0.4	3.8	0.3	100	91.2	1340	50	520	86	51	113	28,700
	Out	73.2	0.6	15.4	3.2	0.05	0.9	0.7	1.0	4.9	0.3	100	96.0	1930	42	196	54	—	124	1760
ATM 005	In	73.2	0.6	20.1	1.5	0.02	0.5	0.3	0.4	3.2	0.2	100	91.4	1300	25	397	78	20	<100	15,200
	Out	72.1	0.6	17.7	3.4	0.03	0.6	0.6	0.5	4.2	0.3	100	89.5	958	39	1060	95	65	<100	11,600
ATM 006	In	69.9	0.6	20.6	1.9	0.05	0.6	1.1	0.5	4.6	0.3	100	90.2	2080	25	405	91	12	105	12,900
	Out	67.2	0.3	17.2	1.9	0.16	0.8	5.7	0.6	5.4	0.7	100	92.7	1790	29	2330	71	49	166	4400
ATM 007	Bulk	71.5	0.4	18.4	1.3	0.03	0.5	2.2	0.7	4.4	0.6	100	91.4	1300	24	9210	118	393	102	8510
ATM 008	In	69.2	0.7	24.2	1.6	0.01	0.5	0.2	0.3	3.2	0.2	100	93.1	1470	33	238	18	17	<100	337
	Out	67.9	0.6	20.0	3.0	0.06	0.9	1.7	0.7	5.0	0.3	100	90.2	1670	64	195	45	—	124	460
ATM 009	In	64.5	0.8	28.5	1.7	0.01	0.6	0.2	0.3	3.2	0.2	100	99.4	1070	49	150	27	8	<100	6900
	Out	71.4	0.7	16.8	3.0	0.05	0.8	1.7	1.0	4.5	0.2	100	93.5	1020	55	391	70	20	115	1060
ATM 010	In	67.8	0.7	24.6	2.0	0.03	0.5	0.3	0.3	3.4	0.3	100	92.4	934	28	4150	62	74	<100	7370
	Out	65.7	0.6	15.6	4.1	0.46	0.5	3.0	2.7	5.1	2.3	100	91.6	2810	34	1520	45	69	245	929
ATM 011	In	68.6	0.7	23.6	1.8	0.03	0.6	0.3	0.4	3.7	0.3	100	97.9	1070	40	986	100	204	112	1000
	Out	74.7	0.6	10.3	2.7	0.39	0.7	4.0	0.8	5.1	0.8	100	91.4	3800	24	1830	42	7	205	445
ATM 012	Bulk	71.6	0.6	19.0	1.7	0.06	0.6	1.6	0.7	3.9	0.3	100	89.5	1800	30	877	69	44	121	8170
ATM 013	In	70.4	0.6	19.9	2.0	0.06	0.7	1.1	0.5	4.5	0.3	100	91.8	2040	73	453	64	5	107	7670
	Out	69.6	0.3	17.9	1.8	0.11	0.7	3.1	0.8	5.3	0.3	100	96.0	1640	29	5040	88	165	130	4620
ATM 014	In	68.1	0.8	23.4	2.0	0.02	0.6	0.4	0.5	4.1	0.2	100	90.4	1160	55	681	59	54	116	10900
	Out	69.5	0.6	13.3	3.9	0.45	0.7	3.8	0.9	6.3	0.5	100	94.6	1870	79	1810	34	49	152	474
ATM 015	Bulk	72.5	0.6	19.2	1.8	0.03	0.7	0.5	0.5	3.9	0.3	100	88.8	1350	29	138	81	37	<100	7980
ATM 016	Bulk	66.9	0.8	23.4	2.1	0.02	0.6	1.4	0.4	4.1	0.3	100	89.6	1190	56	770	50	100	131	18,300
ATM 017	In	71.3	0.8	20.4	2.1	0.04	0.5	0.5	0.5	3.6	0.3	100	91.4	1130	49	204	60	16	107	12,400
	Out	69.4	0.4	17.5	1.8	0.25	0.8	4.4	0.6	4.6	0.4	100	93.5	1710	18	328	50	27	214	3180
ATM 018	In	71.1	0.6	19.8	1.8	0.05	0.6	1.1	0.4	4.2	0.3	100	92.8	2190	36	304	47	—	103	7350
	Out	72.6	0.8	12.9	2.5	0.14	0.8	3.5	0.7	5.7	0.4	100	91.0	1520	58	713	37	—	171	570
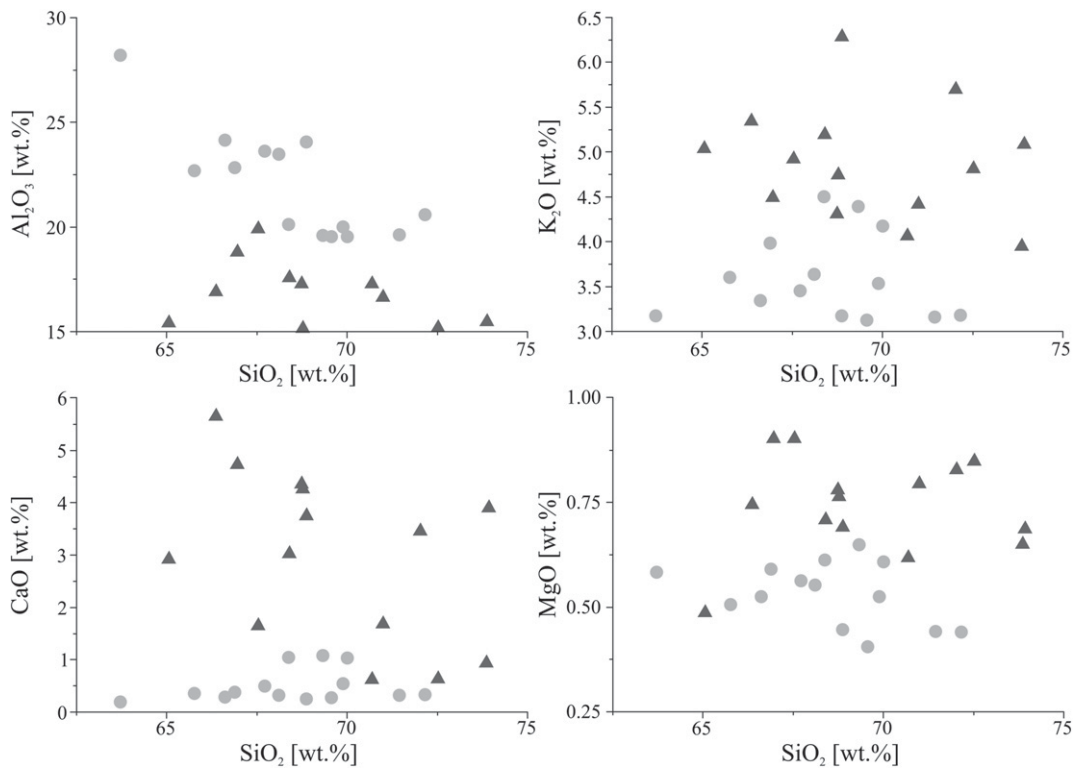
Fig. 8. Diagrams of selected XRF data points allowing a distinct separation related to Al_2O_3, MgO, CaO and K_2O in the main layers (inner layer − dots; outer layer − triangles).
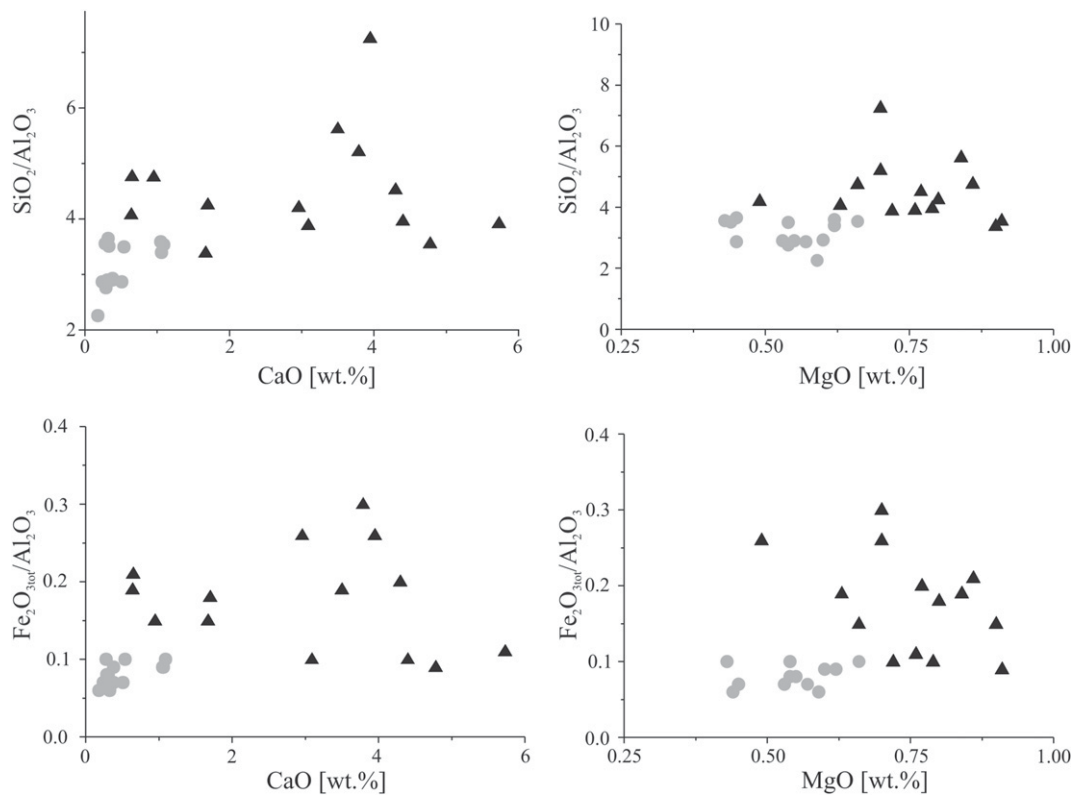

Fig. 9. Binary diagrams of SiO_2/Al_2O_3 and Fe_2O_{3tot}/Al_2O_3 ratios plotted against CaO and MgO indicating no linear dependence between the inner and the outer layer (inner layer − dots; outer layer − triangles).
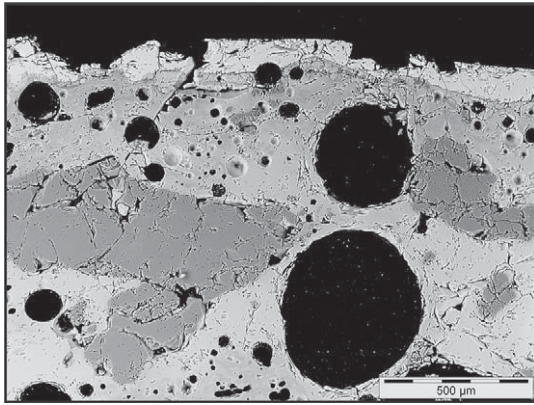
Fig. 10. BSE image of the vitrified engobe and the ceramic inner layer of the crucible ATM 002.

migration within the inner layer. Both, SEM-EDS and EMPA (Table 3) deliver enriched amounts of calcium, potassium and silicon with respect to the inner layer. In general, the results indicate a similar composition like the outer layer except of temper grains, which are missing in the engobe. The instability under the electron beam also indicates a predominantly vitrified character of this layer. Generally, these results favour a similar raw material like the matrix material of the outer layer. Therefore we assume that this engobe is neither the result of migration processes nor formed during use. This layer is rather an added layer with protecting function than a layer formed by chance. One important indication for this theory is the consistent existents of this engobe from the bottom to the top of the crucibles with almost the same composition in several investigated fragments.

4.3. Multiple usages

An indicator for multiple usages is given by the ceramic material itself. Clearly visible repair marks on the outer layer are present in some of the investigated crucible sherds. These are characterised by a duplication of the outer layer, which is marked by the multiplication of the reddish coloured surfaces. The internal composition, structure and main element chemistry of these both layers is almost identical. Thus, we assume an identical raw material used for the primary outer layer and the added one. The overall implication is that the crucible itself was used at least two times.

Preliminary microprobe analyses on preserved metal particles give a hint for multiple usages, too. In general, there are two kinds of alloys found in single crucibles, Cu–Zn and Cu–Sn, with minor traces of iron and lead (unpublished results).

Fig. 11. High-silica part of the SiO_2–K_2O–Al_2O_3 phase diagram (modified after Osborn, 1977; Maggetti et al., 2010). Isotherms are shown every hundred degrees; temperatures in °C. The fat dotted line is the projection toward the mullite-silica cotectic line. The grey dots correspond to the inner layer and the black triangles to the outer layer.

4.4. Estimation of firing temperatures

For the discrimination of a certain firing temperature interval, a combination of different methods had to be used. XRD analyses which represent the coexistence of various mineral phases serve as an indicator for reached temperature ranges. According to Lee et al. (1999), elongated mullite needles develop between 1100 and 1200 °C and diminish the amount of previously formed spinel. The crystallisation of cristobalite from an amorphous silicate-rich phase starts at temperatures above 1300 °C. This minimum temperature can also favour the coexistence of orthorhombic mullite ($Al_6Si_2O_{13}$) and cristobalite (Gualtieri et al., 1995; Lee et al., 1999).

The sum of SiO_2, Al_2O_3 and K_2O yields between 90 and 96%, which allows us to use the ternary SiO_2–K_2O–Al_2O_3 phase diagram to estimate the maximum stability temperatures of the investigated ceramics. The residual 4–10% are mainly attributed to CaO containing additives, which were used to lower the breakdown temperature of the outer layer. In general, the inner layer is characterised by a significant higher amount of Al_2O_3 compared to the outer layer, which corresponds to a higher amount of kaolinitic clay and therefore a high amount of mullite in the ceramic (Fig. 11).

Table 3
EMPA data of the engobe of three different crucibles.

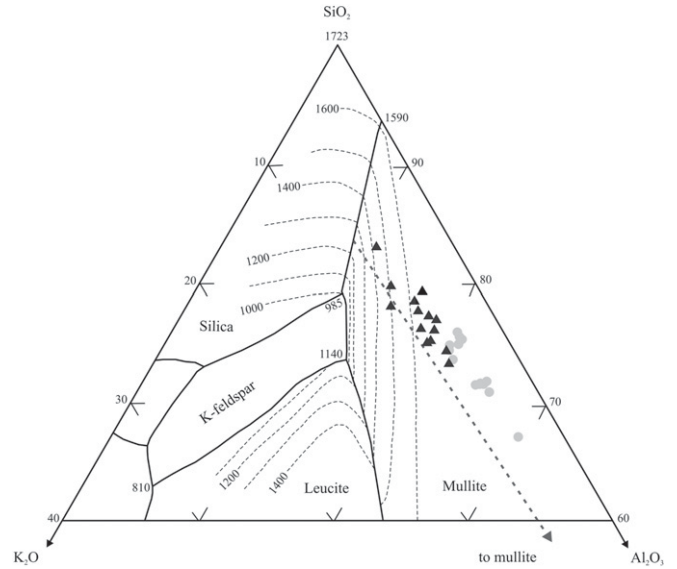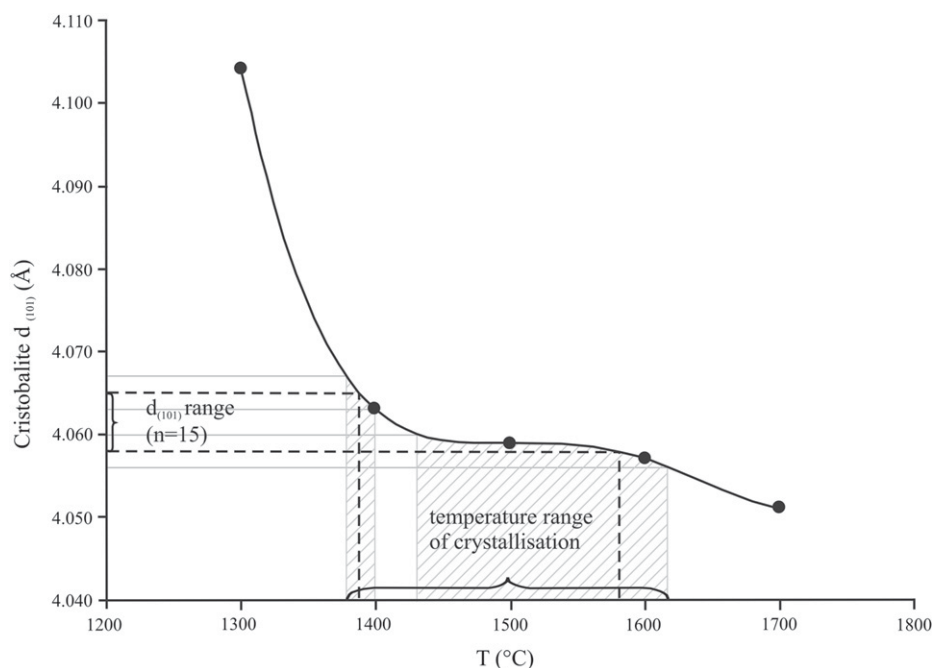| Sample	SiO_2 (wt.%)	TiO_2 (wt.%)	Al_2O_3 (wt.%)	Fe_2O_{3tot} (wt.%)	MnO (wt.%)	MgO (wt.%)	CaO (wt.%)	Na_2O (wt.%)	K_2O (wt.%)	P_2O_5 (wt.%)	CuO_{tot} (wt.%)	SnO_{tot} (wt.%)	ZnO (wt.%)	Total
ATM 002	52.78	0.77	23.40	1.87	0.23	0.95	7.81	1.16	8.04	0.16	–	0.02	3.76	100.94
ATM 002	53.15	0.72	22.51	1.73	0.32	0.99	8.19	1.07	8.51	0.45	–	0.02	3.31	100.98
ATM 002	54.58	0.69	22.09	1.26	0.32	0.96	8.03	1.12	9.04	–	0.08	–	2.44	100.61
ATM 002	52.68	0.74	23.27	1.71	0.32	0.94	8.51	1.11	8.43	0.44	–	–	2.79	100.94
ATM 002	53.80	0.57	20.84	2.76	0.22	1.21	7.19	1.06	8.04	0.74	–	–	3.63	100.05
ATM 002	55.40	0.54	19.68	2.82	0.27	1.25	6.77	1.07	8.23	0.54	–	–	4.11	100.68
ATM 002	55.94	0.45	16.33	1.93	0.28	1.12	11.52	0.90	5.95	0.74	–	0.01	5.04	100.19
ATM 004	48.12	0.17	31.92	0.52	0.03	0.17	15.22	1.36	1.22	0.40	0.54	0.03	1.18	100.87
ATM 004	45.55	0.43	34.19	1.29	0.08	0.81	1.00	1.98	5.94	0.18	–	0.02	9.15	100.62
ATM 004	48.90	0.77	11.86	3.35	0.83	2.17	16.94	1.27	3.30	–	0.20	0.04	10.59	100.22
ATM 012	57.11	0.61	16.43	0.63	0.45	2.02	15.24	2.12	4.68	–	0.01	–	1.02	100.33
ATM 012	54.39	0.65	15.34	0.38	0.54	2.30	20.91	1.00	3.36	0.28	0.72	–	0.60	100.48
ATM 012	55.42	0.60	16.22	0.19	0.53	2.28	20.31	1.04	3.39	0.13	0.32	–	0.25	100.68
ATM 012	57.34	0.77	17.85	0.71	0.39	1.80	12.61	2.08	5.51	0.43	0.20	0.01	1.01	100.72

Fig. 12. Variation curve of the cristobalite $d_{(101)}$ peak as a function of temperature (after Eramo, 2005). The dotted lines show the $d_{(101)}$ range of the crucibles in 15 samples as well as the corresponding range of formation temperature. The grey shaded area displays the error of the peak position.

Cristobalite and tridymite are high temperature − low pressure silica polymorphs. It is generally accepted that pure silica systems do not generate tridymite as a stable phase (Hill and Roy, 1958; Holmquist, 1961; Stevens et al., 1997). The SiO_2 transformation is thus not only a function of pressure and temperature, but composition. Stevens et al. (1997) argued that sodium or potassium carbonate additives can favour the formation of tridymite in SiO_2 rich ceramics. However, despite traces of potassium and sodium, tridymite is missing in all samples. Recent works of Artioli et al. (2008) and Pradell et al. (2010) have demonstrated that tridymite formation is related to the existence of stabilising alkali ions, but, the differences in the reached temperatures and pressures are in fact also important. The phase transition of α-quartz to β-cristobalite in pure silica systems occurs above temperatures of 1400 °C with an intermediate amorphous phase (Stevens et al., 1997). Multi-element/-mineral ceramics as presented here tend to influence such reaction temperatures and probably resulting in lower temperatures of such phase transitions. Due to the fact that the crystalline order of cristobalite is increasing with temperature (Eramo, 2005; Sosman, 1965; Verduch, 1958), it is possible to use the $d_{(101)}$ peak range as a temperature indicator, which shifts to lower d-values as the formation temperatures increase (Eramo, 2005; Verduch, 1958). The $d_{(101)}$ cristobalite peak positions of 15 crucibles (Fig. 12) lie in the range of 0.4058−0.4065 nm (±0.0002 nm), which correspond to firing temperatures above 1380 °C.

In addition, the amount of analcime, which is a secondary devitrification product of potassium- and sodium-rich glassy phases under humid and acidic environmental conditions in the burial stage, can be used as indicator for firing temperatures higher than 1200 °C. In general, the amount of analcime increases with increasing firing temperature (Buxeda et al., 2002; Pradell et al., 2010; Schwedt et al., 2006).

All these data indicate firing temperatures higher than necessary for the production of α-brass with melting point of around 1000−1050 °C. Nevertheless, the mineral assemblage indicates firing temperatures between 1200 and 1400 °C, i.e. much higher than the necessary melting temperature. Such an overheating

might be necessary to melt the load in large crucibles as shown in Fig. 2 in a moderate period of time. Moreover, it enables a longer handling of the molten content to produce a higher number of small artefacts like fibulae. Indications for such a high overheating are present in all investigated crucible fragments. This fact demonstrates the skills of Roman craftsmen which enabled them to produce in an "industrial" way, i.e. consistent production of a high quantity of crucibles and metal artefacts during decades.

5. Conclusion

Summing up, the results of this work demonstrate that all investigated crucibles are double-layered with clear mineralogical and structural differences in individual layers. Owing to differences in the feldspar-quartz proportions of the temper grains, it is possible to propose a granitic source for the raw material. The matrix of both layers consists of kaolinitic clay with high refractory characteristics. Only the outer layer has an additive which reduces the refractory performance of the matrix material, thus increasing the insulation function of the layer. The detected engobe consists of a material nearly identical to the matrix of the outer layer. It delays the migration of a liquid metal charge, giving it a protecting function and avoiding metal losses.

Clear evidence for a multiple usage were presented based on partial duplication of the outer layer as well as varying metal compositions of the metal droplets in single crucibles. The applied cristobalite peak method and temperature estimation derived from the mineral assemblage suggest relatively high firing temperatures (≥1380 °C). This range is generally higher than temperatures described for Roman metal-melting crucibles in literature (Freestone, 1989; Hein et al., 2007; Rehren, 2003; Tylecote, 1982). However, such high pre-firing temperatures are already reported from a 15th/16th century excavation in Hesse/Germany (Martinón-Torres et al., 2008) and from the 17th century glass-melting crucibles from Derrière Sairoche/Switzerland (Eramo, 2006).

Overall, the crucibles were produced using a certain routine, which seems to be identical for all analysed fragments. At first the

inner layer was built up of kaolinitic clay and a granite-related temper. This layer has been dried or fired at low temperatures. Afterwards, the outer layer consisting of a different kind of clay with a higher calcium content and granitic temper was added. The engobe was probably produced simultaneously by elutriate the clay of the outer layer and dispersing this suspension along the inner layer of the crucible which initially led to a millimetre thin layer covering the whole inside. Subsequent firing created a glassy engobe and outer layer with a ceramic inner layer in-between. Thus, the used production routine seems to be an appropriate method to produce crucibles stable under high temperature and suited for a multiple use.

Acknowledgements

References

Artioli, G., Angelini, I., Polla, A., 2008. Crystals and phase transitions in protohistoric glass materials. Phase Transitions 81, 233−252.

Bayley, J., 1992. Metalworking ceramics. Medieval Ceramics 16, 3−10.

Bayley, J., Rehren, Th, 2007. Towards a functional and typological classification of crucibles. In: La Niece, S., Hook, D., Craddock, P.T. (Eds.), Metals and Mines − Studies in Archaeometallurgy. Archetype, London, pp. 46−55.

Buxeda, J., Mommsen, H., Tsolakidou, A., 2002. Alterations of Na, K and Rb concentrations in Mycenaean pottery and a proposed explanation using X-ray diffraction. Archaeometry 44, 187−198.

Chardron-Picault, P., Pernot, M., 1999. Un quartier antique d'artisanat métallurgique à Autun- Le site du Lycée militaire. Editions de la Maison des sciences de l'homme. Documents d'Archéologie Française 76, Paris.

Eramo, G., 2005. The melting furnace of the Derrière Sairoche glassworks (Court, Swiss Jura): heat-induced mineralogical transformations and their technological signification. Archaeometry 47, 571−592.

Eramo, G., 2006. The glass-melting crucibles of Derrière Sairoche (1699−1714 AD, Ct. Bern, Switzerland): a petrological approach. Journal of Archaeological Science 33, 440−452.

Freestone, I.C., 1989. Refractory materials and their procurement. In: Hauptmann, A., Pernicka, E., Wagner, G. (Eds.), Old World Archaeometallurgy. Der Anschnitt, Beiheft 7. Deutsches Bergbau-Museum, Bochum, pp. 155−162.

Gualtieri, A., Bellotto, M., Artioli, G., Clark, S.M., 1995. Kinetic study of the kaolinite-mullite reaction sequence. Part II: mullite formation. Physics and Chemistry of Minerals 22, 215−222.

Hein, A., Kilikoglou, V., Kassianidou, V., 2007. Chemical and mineralogical examination of metallurgical ceramics from a Late Bronze Age copper smelting site in Cyprus. Journal of Archaeological Science 34, 141−154.

Hill, V.G., Roy, R., 1958. Silica structure studies, VI, on tridymite. Transactions of the British Ceramic Society 57, 496−510.

Holmquist, S.B., 1961. Conversion of quartz to tridymite. Journal of the American Ceramic Society 44, 82−86.

Lee, W.E., Iqbal, Y., 2001. Influence of mixing on mullite formation in porcelain. Journal of the European Ceramic Society 21, 2583−2586.

Lee, S., Kim, Y.J., Moon, H., 1999. Phase transformation sequence from kaolinite to mullite investigated by energy-filtering transmission electron microscope. Journal of the American Ceramic Society 43, 2841−2848.

Maggetti, M., Kahr, G., 1980. Homogenität archäologischer keramischer Objekte: Teil I. Porosität und Porenradienverteilung. Archäologie und Naturwissenschaften 2, 1−20.

Maggetti, M., Rosen, J., Neururer, C., Serneels, V., 2010. Paul-Louis Cyfflé's (1724−1806) Terre de Lorraine: a technological study. Archaeometry 52, 707−732.

Martinón-Torres, M., Freestone, I., Hunt, A., Rehren, Th, 2008. Mass-produced mullite crucibles in medieval Europe: manufacture and material properties. Journal of the American Ceramic Society 91, 2071−2074.

Modarressi-Tehrani, D., 2004. Ein Ensemble frühlatènezeitlicher Metallverarbeitung aus der Siedlung von Eberdingen-Hochdorf (Lkr. Ludwigsburg). Metalla 11.1, Bochum.

May, J.O., Butterworth, B., 1962. Studies of pore size distribution III. The effect of firing temperatures. Science of Ceramics 1, 201−221.

Nielen, H.-D., 2006. Zink oder Messing? Ein Beitrag zu den metallurgischen Tätigkeiten im Legionslager Neuss. Metalla 13.1, Bochum.

Osborn, E.F., 1977. Phase-diagrams and refractories. American Ceramic Society Bulletin 56, 654−659.

Pradell, T., Molera, J., Salvado, N., Labrador, A., 2010. Synchrotron radiation micro-XRD in the study of glaze technology. Applied Physics A-Materials Science & Processing 99, 407−417.

Rehren, Th, 2003. Crucibles as reaction vessels in ancient metallurgy. In: Craddock, P.T., Lang, J. (Eds.), Mining and Metal Production Through the Ages. British Museum Press, London, pp. 207−215.

Schwedt, A., Mommsen, H., Zacharias, N., Buxeda, J., 2006. Analcime crystallization and compositional profiles − comparing approaches to detect post-depositional alterations in archaeological pottery. Archaeometry 48, 237−251.

Sosman, R.B., 1965. The Phases of Silica. Rutgers University Press, New Brunswick, New Jersey.

Stevens, S.J., Hand, R.J., Sharp, J.H., 1997. Polymorphism of silica. Journal of Material Science 32, 2929−2935.

Thornton, C.P., Rehren, Th, 2009. A truly refractory crucible from fourth millennium Tepe Hissar, Northeast Iran. Journal of Archaeological Science 36, 2700−2712.

Tite, M.S., Freestone, I.C., Meeks, N.D., Craddock, P.T., 1985. The examination of refractory ceramics from metal-production and metalworking sites. In: The Archaeologist and the Laboratory. Council for British Archaeology Research Report 58, pp. 50−55.

Tylecote, R.F., 1982. Metallurgical crucibles and crucible slags. In: Olin, J.S., Franklin, A.D. (Eds.), Archaeological Ceramics. Smithsonian Institution Press, Washington, pp. 231−243.

Verduch, A.G., 1958. Kinetics of cristobalite formation from silicic acid. Journal of the American Ceramic Society 41, 427−432.